Adaptation of Human Parainfluenza Virus to Airway Epithelium Reveals Fusion Properties Required for Growth in Host Tissue

Samantha G. Palmer,[a] Matteo Porotto,[a] Laura M. Palermo,[a] Luis F. Cunha,[b] Olga Greengard,[a,c] and Anne Moscona[a]

Departments of Pediatrics and Microbiology and Immunology, Weill Medical College of Cornell University, New York, New York, USA[a]; Human Oncology and Pathogenesis Program, Memorial Sloan-Kettering Cancer Center, New York, New York, USA[b]; and Department of Pediatrics, Mount Sinai School of Medicine, New York, New York, USA[c]

ABSTRACT **Paramyxoviruses, a family of RNA enveloped viruses that includes human parainfluenza virus type 3 (HPIV3), cause the majority of childhood croup, bronchiolitis, and pneumonia worldwide. Infection starts with host cell receptor binding and fusion of the viral envelope with the cell membrane at the cell surface. The fusion process requires interaction of the two viral surface glycoproteins, the hemagglutinin-neuraminidase (HN) and the fusion protein (F). We have previously shown that viruses with an HN/F pair that is highly fusogenic in monolayers of immortalized cells due to mutations in HN's secondary sialic acid binding site are growth impaired in differentiated human airway epithelium (HAE) cultures and *in vivo*. Here we have shown that adaptation of HPIV3 to growth in the lung is determined by specific features of HN and F that are different from those required for growth in cultured immortalized cells. An HPIV3 virus bearing a mutated HN (H552Q), which is fit and fusogenic in immortalized cells but unfit for growth in the lung, evolved into a less-fusogenic but viable virus in differentiated human airway epithelium. Stepwise evolution led to a progressive decrease in efficiency of fusion activation by the HN/F pair, with a mutation in F first decreasing the activation of F by HN and a mutation in HN's secondary sialic acid binding site decreasing fusion activation further and producing a stable virus. Adaptation of HPIV3 to successful growth in HAE is determined by specific features of HN and F that lead to a less easily activated fusion mechanism.**

IMPORTANCE **Human parainfluenza viruses (HPIVs) are paramyxoviruses that cause the majority of childhood cases of croup, bronchiolitis, and pneumonia worldwide, but there are currently no vaccines or antivirals available for treatment. Enveloped viruses must fuse their membrane with the target cell membrane in order to initiate infection. Parainfluenza virus fusion proceeds via a multistep reaction orchestrated by the two glycoproteins that make up its fusion machine. The receptor-binding hemagglutinin-neuraminidase (HN), upon receptor engagement, activates the fusion protein (F) to penetrate the target cell and mediate viral entry. In this study, we show that the precise balance of fusion activation properties of these two glycoproteins during entry is key for infection. In clinically relevant tissues, viruses evolve to acquire a set of fusion features that provide key clues about requirements for infection in human beings.**

Received 4 May 2012 **Accepted** 8 May 2012 **Published** 5 June 2012

Citation Palmer SG, et al. 2012. Adaptation of human parainfluenza virus to airway epithelium reveals fusion properties required for growth in host tissue. mBio 3(3):e00137-12. doi:10.1128/mBio.00137-12.

Editor Diane Griffin, Johns Hopkins University School of Public Health

Address correspondence to Anne Moscona, anm2047@med.cornell.edu.

Human parainfluenza virus 3 (HPIV3) is a major cause of pediatric croup, bronchiolitis, and pneumonia worldwide, and in the United States it accounts for a significant share of pediatric respiratory hospitalizations, as well as a rising number of infections in immunocompromised patients. There are no vaccines or treatments against it or any of the other HPIVs (1–4). HPIVs are enveloped paramyxoviruses, carrying two surface glycoproteins, the hemagglutinin-neuraminidase (HN) and the fusion (F) protein. After binding to the host receptor, sialic acid, HN and F interact to mediate fusion prior to delivery of the viral genome into the host cell. The correct timing of F activation by HN is essential for infection: to be effective, triggering of F to its active state must occur only when F is positioned near the target cell membrane (5).

The HN protein, which is present as a tetramer composed of two dimers on the surface of the virus and the infected cell, performs three important functions during the HPIV3 viral life cycle. In addition to receptor binding, the initial step of entry, and F activation, which promotes the steps of entry after receptor binding, HN has the third function of receptor cleavage, performed by its neuraminidase activity to promote the budding of new viruses from an infected cell. The communication between the two molecules that comprise the paramyxovirus fusion machine is biologically relevant, with impact on infection in the natural host. We have studied HPIV3 virus variants bearing mutations at one of HN's sialic acid receptor binding sites, either in the primary receptor binding site identified in the existing crystal structure or in a secondary sialic acid binding site (site II), present at the dimer interface and required for activation of F (6–8). Alterations in site II at the dimer interface of HPIV3 HN influence growth, implicating HN's site II in pathogenesis (9). The virus HPIV3 HN H552Q, bearing a mutation at HN's site II, binds its receptor more avidly,

activates F more efficiently, fuses in monolayer culture more extensively (6, 7), and physically interacts with F more strongly (10). However, this virus is unfit *in vivo* (cotton rat model) and in human airway epithelium (HAE), a pseudostratified, highly differentiated model of unpassaged primary cells that closely resembles the epithelial tissue of the human respiratory tract (9). This suggests that an increase in F activation efficiency is a disadvantage in the natural host. The virus with enhanced F triggering produces inactive viral particles in HAE, in which the F protein may have been triggered before contacting target cells (9). These HN-F relationships are physiologically relevant (9): too-active HN-F interaction may lead to premature, and therefore ineffective, activation of the fusion process (5).

To obtain experimental support or proof for this notion, we turned to the virus and the process of natural selection: in HAE, which includes a variety of cell types, cilia, and mucus, as in the human lung (11), the site II-mutated variant HPIV3 HN H552Q virus adapted for survival by evolving to decrease the ease of triggering of F and the extent of fusion. We have shown here that infection in lung tissue depends upon a specific balance of fusion activation, determined by both the efficiency of HN at triggering F and the stability of the pretriggered state of F. Viruses with highly efficient F-triggering capacity—whether HN triggers F too efficiently or F is too readily triggered—were not favored in the selection process, likely due to premature triggering of F. The HPIV3 HN H552Q variant virus under the selective pressure of HAE acquired sequential mutations in the F and HN proteins that lowered HN-receptor interaction and lowered F activation, ultimately promoting growth in HAE. The first mutation emerged in the F protein, followed by a mutation in HN's secondary sialic acid binding site. No reversion to the laboratory wild-type (wt) virus was identified. The new HPIV3 variant that emerged during growth of HPIV3 HN H552Q in HAE carries an HN-F fusion apparatus with functional properties that are suited to growth in lung tissue.

RESULTS

Growth of HPIV3 HN H552Q in HAE is ineffective but leads to emergence of plaque size variant viruses. The variant HPIV3 HN H552Q infected HAE cells, but by 3 days it did not produce infectious progeny virions, yielding only noninfectious viral particles (9, 12). To determine whether the selective pressure of HAE would yield a virus suited to growth in HAE, HPIV HN H552Q was grown in HAE for 12 days. Cultures were infected with 4,000 PFU of either HPIV3 wt or HN H552Q, fluids containing released viruses were collected each day postinfection, and titers were determined in cell monolayers (Fig. 1).

Figure 1A outlines the experiment. Infection with HPIV3 wt (blue line) produced infectious titers throughout the experiment, with plaque size remaining unchanged after 12 days. In contrast, infection with HPIV3 HN H552Q (bright red) yielded zero viral titer up to 3 days after infection. At 5 days after infection, a mixed population (brown) of medium-plaque (diameter, 0.39 mm) and small-plaque (diameter, 0.12 mm) viruses was retrieved in replicate experiments, unlike either the large plaques (diameter, 1.08 mm) of the highly fusogenic parental HPIV3 HN H552Q or plaques of HPIV3 wt (diameter, 0.61 mm), as shown in Fig. 1B. By 7 to 9 days after infection, the population contained only small-plaque viruses, at titers greater than those of HPIV3 wt (data not shown), and medium-plaque virus did not reappear. This pattern of emergence of variant viruses consistently reoccurred in each of the seven times that this experimental protocol was carried out.

To assess the growth in HAE of the medium- and small-plaque viruses relative to that of parental HPIV3 HN H552Q, samples were plaque purified and used to infect HAE. Their growth was compared to those of the parent and wild-type viruses (Fig. 1C). As expected, up to 3 days postinfection, HPIV3 HN H552Q yielded zero titer, while the HPIV3 wt produced 10^5 PFU/ml. Infection with the medium-plaque virus yielded up to 10^4 PFU/ml 2 days postinfection, followed by emergence of a mixed population of medium and small plaques, with only small plaques by 7 days postinfection (data not shown). Infection with the small-plaque virus yielded growth up to 3 logs higher than that of HPIV3 wt within the first 3 days of HAE infection, peaking at 10^7 PFU/ml. The HN H552Q variant appears to have undergone sequential alterations that overcame its growth defect in HAE. The associated, progressive decrease in plaque size (Fig. 1B) suggests selection in HAE for viruses with a lower cell fusion capacity.

The high infectious titers attained in HAE by the small-plaque virus relative to those of the wt virus, as well as HPIV3 HN H552Q, might be accounted for by an increase in the number of released virions (total particles). However, quantification by quantitative real-time PCR (qRT-PCR) of the amount of genome retrieved from HAE 3 days after infection for the small-plaque virus was similar to that for wt virus of HPIV3 HN H552Q (Fig. 1D). This similarity permitted calculation of the amounts of infectious virions. On average, 60% of the small-plaque virus population was infectious, as opposed to 15% of the HPIV3 wt population and 0% for the HPIV3 HN H552Q variant (Fig. 1E). Thus, while all three viruses produce particles, the ratio of infectious particles to total particles is higher in the stable small-plaque virus that emerges from the HPIV3 HN H552Q parent in HAE.

Viability of emerging variants is associated with mutations in HN and F envelope glycoproteins. The RNA of the viruses emerging from six different infections of HAE with HPIV3 wt, HN H552Q, the medium-plaque viruses, and the small-plaque viruses was extracted, and the HN and F genes were sequenced (Table 1). Viruses retrieved from HAE infected with HPIV3 wt retained wt HN and F sequences. Noninfectious HPIV3 HN H552Q collected 1 day postinfection carried HN with the H552Q mutation and wild-type F. The medium-plaque virus (the first to appear) carried HN H552Q and F G396D. The small-plaque virus carried the HN H552Q and F G396D mutations, as well as a Q559R mutation in HN. Figure 2A shows the HPIV3 HN dimer structure, with H552Q and Q559 marked; Fig. 2B shows the homology model of the HPIV3 F protein prefusion structure, and the HPIV3 F postfusion structure, with G396 marked. The Q559R HN mutation is located in the secondary sialic acid binding site that is present at the dimer interface and has been implicated in activation of F (7, 13).

Evolution towards slower HN-F triggering and fusion. The failure of the highly fusogenic HPIV3 HN H552Q virus to produce active virions in HAE infection could be due to the premature triggering of the F protein in the progeny virions, leading to inactivation of the virions (9). In this case, positive selection in HAE should favor mutations that overcome this tendency to prematurely trigger F. A quantitative fusion assay was used to evaluate the fusion promotion capacity of each HN-F pair (7, 13, 32). 293T cells coexpressing F wt or F G396D with HN H552Q or HN H552Q,Q559R were overlaid with receptor-bearing cells at 37°C

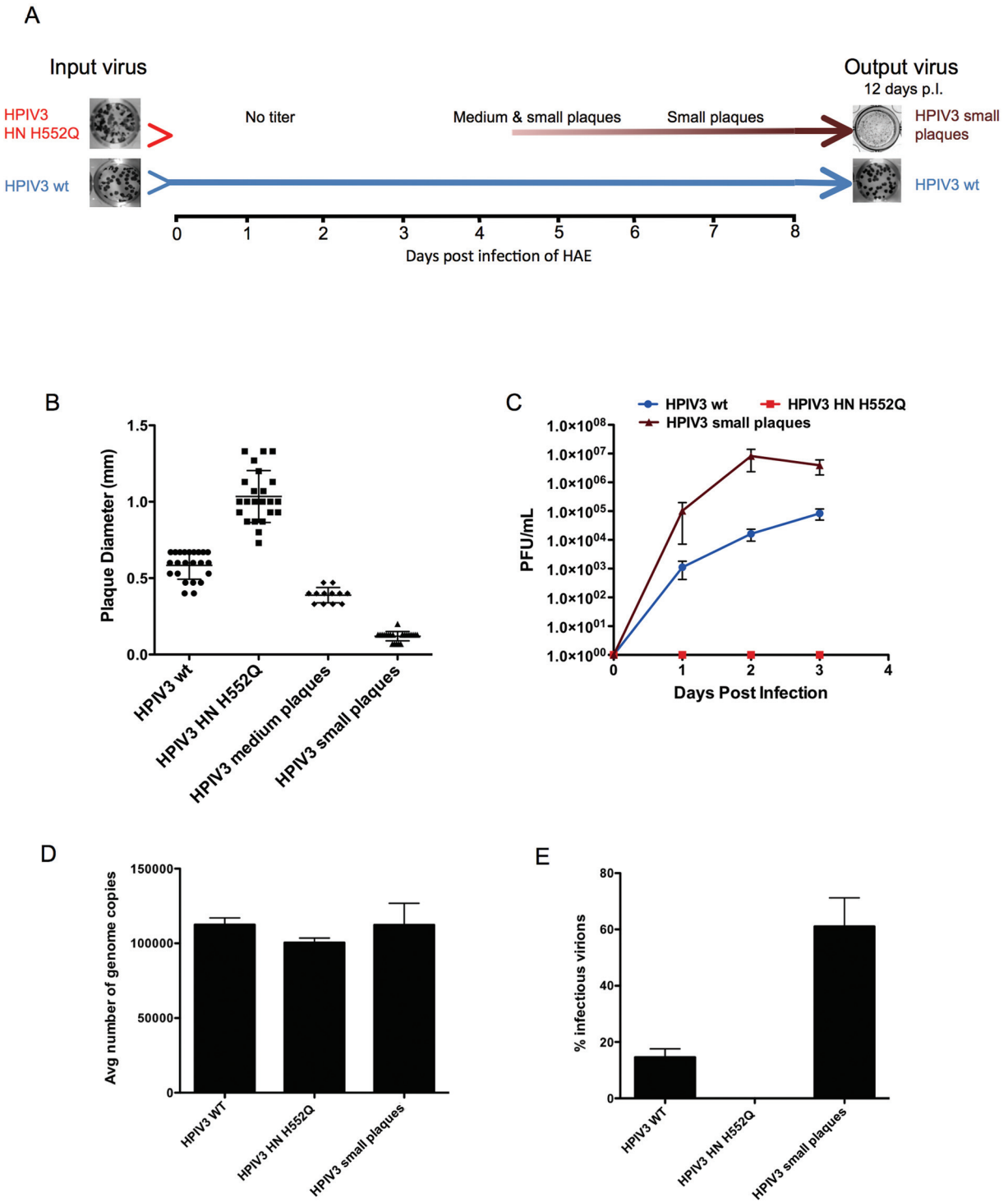

FIG 1 HAE infection with HPIV3 HN H552Q: emergence of variants. (A) Timeline of viral growth after infection of HAE with wt HPIV3 (blue) and HPIV3 HN H552Q (red). (B) Plaque diameter in CV1 cells 16 to 18 h after infection with the indicated virus retrieved from HAE ($n = 20$ per virus from 3 experiments). (C) Titers of viruses grown in HAE: wt HPIV3 (blue), HPIV3 HN H552Q (red), or HPIV3 "small plaques" (brown). Data points are means (±SD) of triplicate measurements and are representative of at least 5 experiments. (D) Quantitation of viral genome released 3 days post-HAE infection (determined by qRT-PCR). Data points are means (±SD) of triplicate experiments. (E) Percentage of infectious virions (out of total particles) retrieved from infection of HAE.

for 3 h, and fusion was measured. As observed with plaque sizes (Fig. 1B), fusion is reduced if F G396D (instead of wt F) is paired with HN H552Q. Fusion decreased by 32% when wt F is replaced with F G396D, indicating that the mutation G396D produced less fusion in the presence of the same H552Q HN (Fig. 3A). With the second HN mutation (H552Q Q559R), the fusion capacity de-

TABLE 1 Mutations acquired in HN and F glycoproteins of HPIV3 variants

HPIV3 variant	HN mutation(s)	F mutation
HN H552Q	H552Q	None
Medium-plaque virus	H552Q	G396D
Small-plaque virus	H552Q, Q559R	G396D

creases more, indicating that the Q559R mutation in HN also decreased the efficiency of the HN-F fusion pair.

Specific HN-F-triggering efficiency was assessed using a fusion-triggering assay to determine the temperature of F activation for each HN-F pair. Cells coexpressing the indicated HN and F pair (Fig. 3B) were allowed to bind erythrocytes (RBCs) at 4°C. The cells were then washed to remove unbound RBCs and transferred to fresh medium at 4, 15, 22, 30, or 37°C for 1 h, to allow F activation. The amount of target RBCs that (i) were released into the medium by HN's innate neuraminidase activity (dotted line), (ii) were bound but had not fused (dashed lines), or (iii) had undergone fusion (solid lines) was determined. The temperature of F activation (defined as the temperature for 50% RBC fusion) increased from 12°C for HN H552Q with F wt to 29°C for HN H552Q with F G396D (medium plaques), indicating that the F mutant requires more heat energy to be activated than does F wt in the presence of the same HN (Fig. 3B). The virus yielding stable and infectious small plaques, bearing HN H552Q,Q559R and F G396D, had the highest temperature requirement (>37°C) for F activation, achieving only 20% fusion at 37°C. The final extent of fusion accomplished by this HN/F pair is also affected by the significant amount of release of RBCs from the expressing cell surfaces; this issue will be further addressed below (see Fig. 5C).

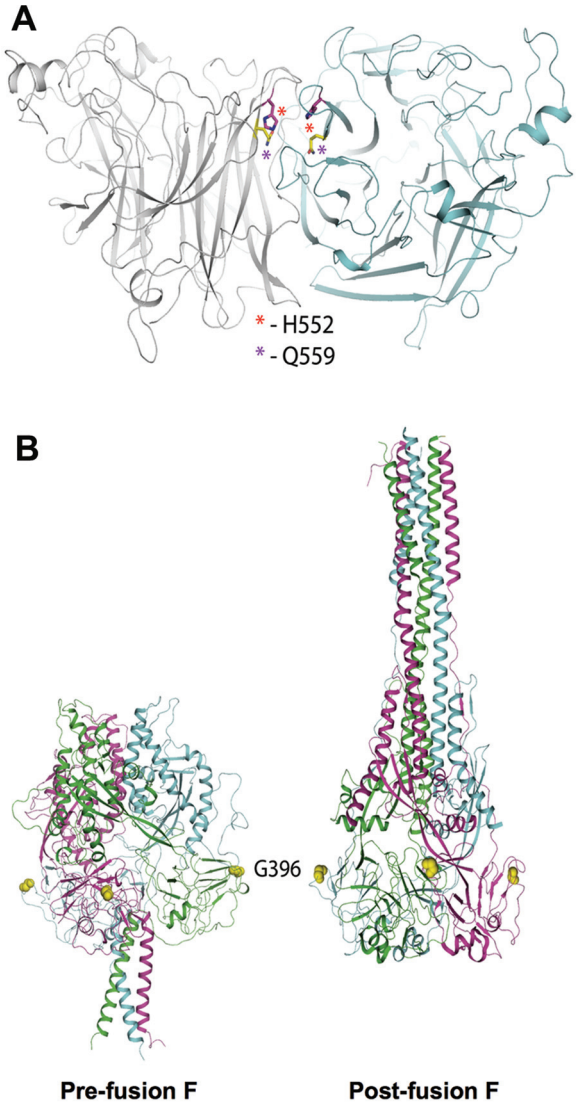

FIG 2 Molecular structure of wild-type and mutant HN and F. (A) HN dimer structure (PDB IV2I), with the monomers colored gray and cyan. The locations of the H552Q and Q559R mutations at the dimer interface are highlighted by showing residues H552 and Q559 as sticks and marked with asterisks. The structure was subjected to 20 ns of MD simulation. (B) Crystal structure of the postfusion HPIV3 F protein (right) and a homology model of the prefusion protein, based on PIV5 F (left). The three chains of F are colored green, cyan, or magenta. The G396 residues are represented as yellow spheres.

The mutation G396D confers slower activation kinetics of the F protein. The effect of the G396D mutation in F could result from less-efficient triggering or from less-effective fusion promotion after triggering. To distinguish between these two possibilities, heat activation of wt F and mutant F G396D in the absence of HN was carried out. Hemagglutinin (HA) can be used to bind to receptor-bearing cells that are targets for HPIV3 F-mediated fusion; since influenza virus HA and HPIV3 F do not interact on the cell surface and HA does not trigger F to mediate fusion (10), HA serves simply to cause the cells to adhere. Cells were transfected with influenza virus HA with either wt F or mutant F G396D, the cells were incubated at 45°C to activate F (14, 15), and fusion was measured over time (Fig. 4). At 30 min, F G396D showed approximately 18% less fusion than F wt. By 60 min there was no significant difference in the fusion between F wt and F G396D, indicating that F G396D was less efficient at initial activation but once activated was fully fusion competent.

Mutations acquired in HN's secondary sialic acid binding site ("site II") lower avidity. To dissect the role of the HN Q559R mutation in the secondary sialic acid binding site, HNs bearing both H552Q and Q559R were compared with each singly mutated HN and wt HN for receptor avidity, neuraminidase, and F-triggering properties. To measure receptor binding avidity, cells transiently expressing either of the four HNs were pretreated with neuraminidase to remove receptors on the expressing cells' surfaces and eliminate potential interactions between HN and receptor molecules on the HN-expressing cell surface (7). Aliquots of RBCs with graded receptor depletion were then used to quantify RBC binding to the HNs; HN molecules with higher avidity bind RBCs that have lower receptor density (higher depletion). As expected, HN H552Q showed higher avidity than HN wt (50% binding to RBCs treated with 54 mU of neuraminidase, compared to 50% binding to RBCs treated with 44 mU neuraminidase) (Fig. 5A). For HN H552Q,Q559R, avidity is markedly reduced (50% binding at 19 mU neuraminidase). This decrease can be accounted for by the Q559R mutation, which singly (HN Q559R) showed 50% binding at 17 mU of neuraminidase. The strikingly reduced avidity conferred by Q559R points to the role of the secondary sialic acid binding site in receptor avidity.

The Q559R mutation also impacted HN's neuraminidase activity, known to reside in site I. Neuraminidase activity of the doubly mutated HN H552Q,Q559R was approximately 80% of

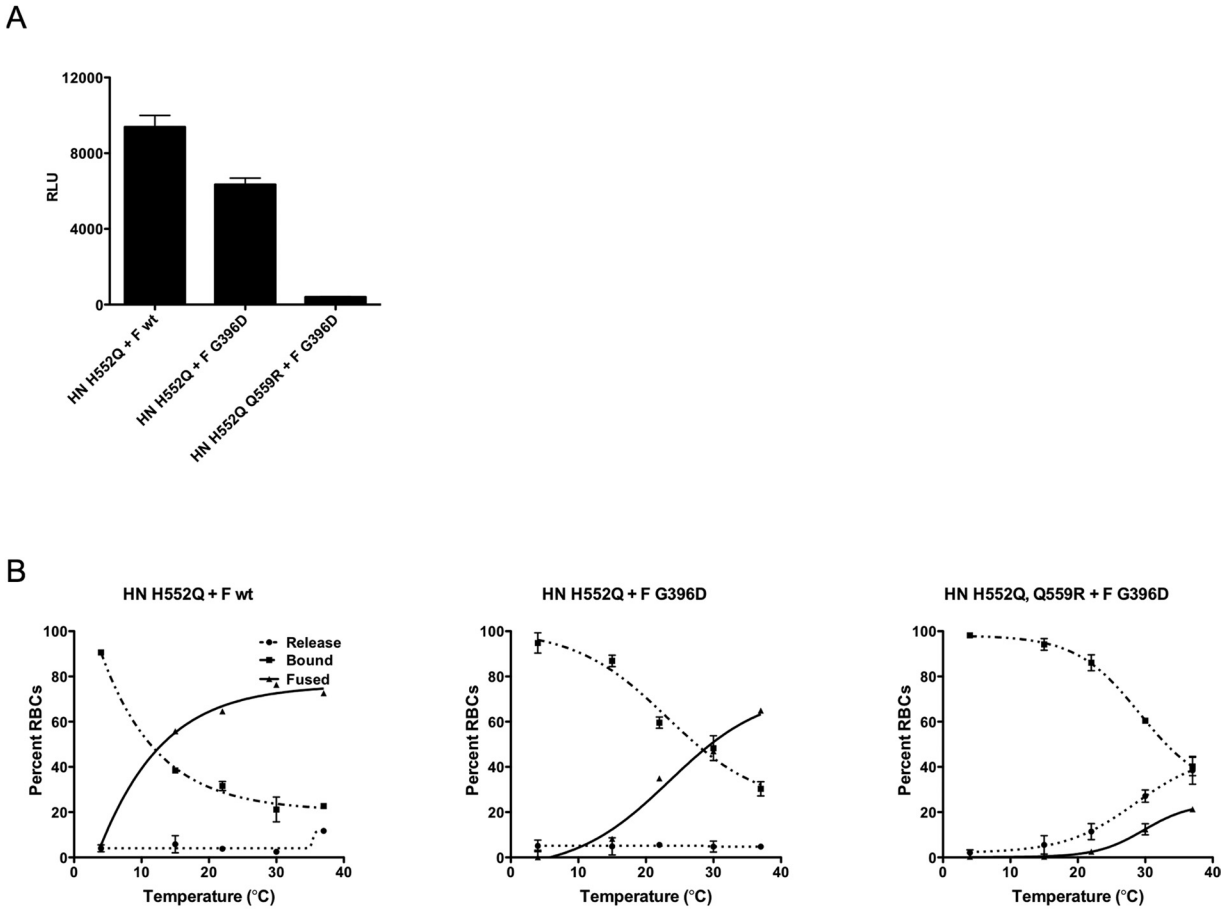

FIG 3 Cell fusion promoted by parental and mutant glycoproteins. (A) Cell-cell fusion mediated by the indicated HN-F pairs was quantitated after 3 h at 37°C using a beta-galactosidase complementation assay. The bars represent means ± SD of data from at least 3 experiments. (B) 293T cells coexpressing the indicated HN-F pair were allowed to bind RBCs at 4°C and then transferred to 4, 15, 22, 30, or 37°C for 1 h. Released, bound, and fused RBCs were quantified. The values are means (±SD) of results from three experiments.

that of parental HN H552Q (see Table 2). This is likely to be due to an allosteric effect on site I, but this remains to be explored mechanistically. Since both the binding and neuraminidase activities of HN were affected by the Q559R mutation, we hypothesized that the duration of receptor engagement may be shorter for the small-plaque virus' HN than for parental HN H552Q. To address this question, the time course of each HN's binding and releasing sialic acid receptors was determined at 37°C. Cells expressing HN WT, HN H552Q, HN H552Q,Q559R, or HN Q559R were incubated with 1% RBC suspensions for 30 min at 4°C, rinsed to remove unbound RBCs, and transferred to 37°C. At the indicated time points (Fig. 5B), the released and bound RBCs were collected and quantified. Within 15 min of incubation at 37°C, approximately 44% and 47% of RBCs were released from HN H552Q,Q559R and HN Q559R, respectively, compared to only 13% for HN wt and 0.7% for HN H552Q. This faster receptor detachment from HN H552Q,Q559R and HN Q559R reflects the lower ratio of receptor avidity to neuraminidase activity for these variant HNs than for parental HN H552Q.

Mutations acquired in HN's site II impair HN's F-triggering ability. To address the effect of Q559R on HN's F activation property, the fusion-triggering assay was carried out with HN wt, HN H552Q,Q559R, or HN Q559R coexpressed with F wt. Again the

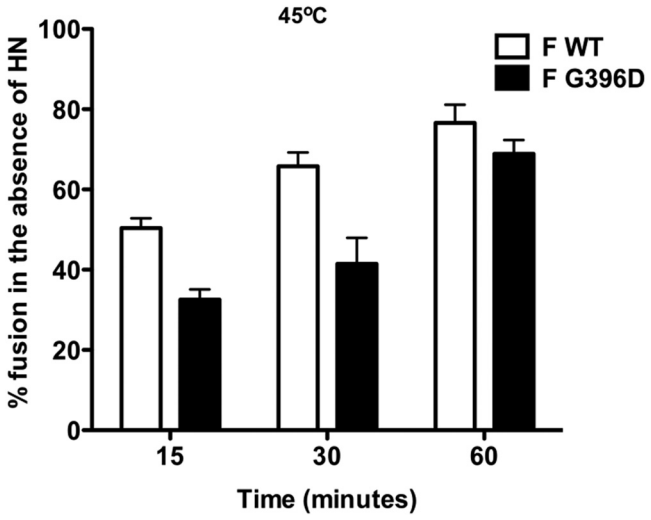

FIG 4 Activation kinetics of F wt and F G396D in the absence of HN at 45°C. 293T cells transiently expressing influenza virus HA and either F wt or F G396D were overlaid with RBCs at 45°C for 60 min. The percent RBCs fused (*y* axis) over time (*x* axis) was quantified. The values are means (±SD) of results from three experiments.

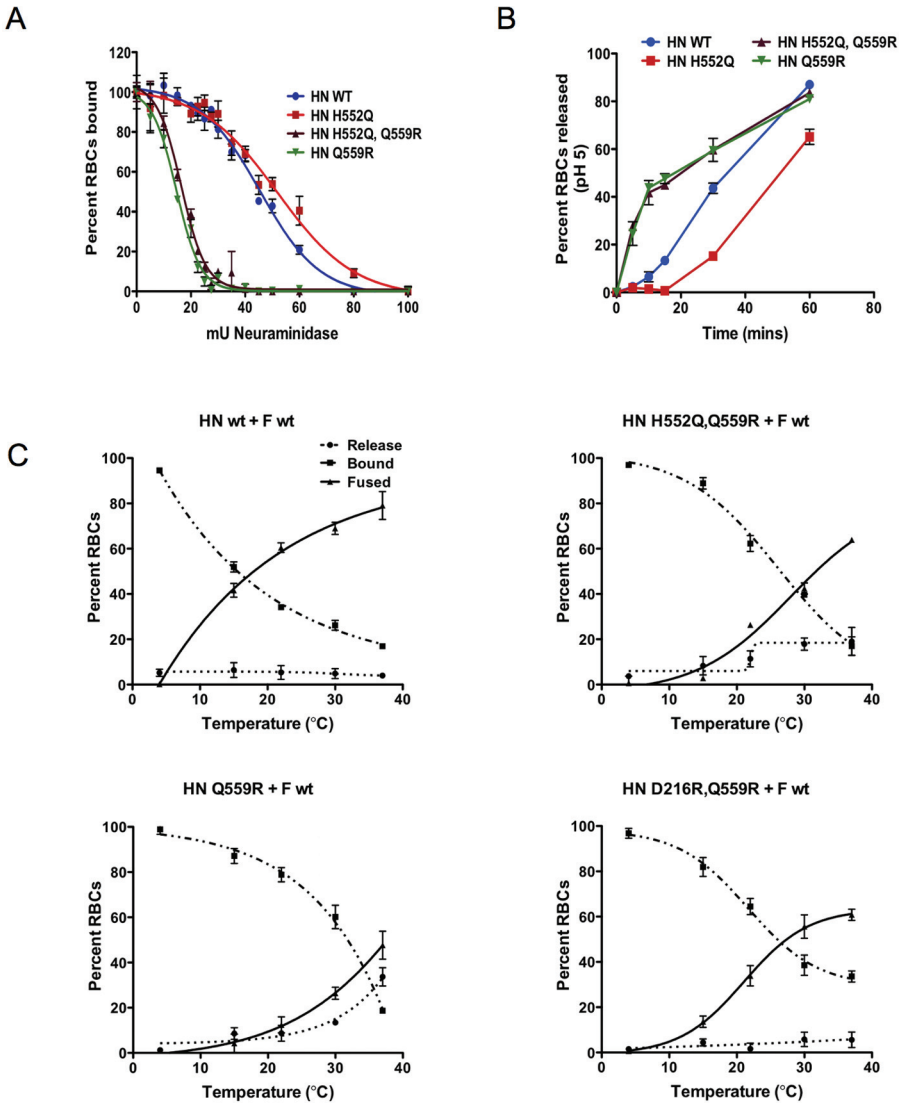

FIG 5 Effects of HN mutation on avidity, neuraminidase, receptor release, and F activation. (A) A panel of RBCs with different degrees of receptor depletion was used to quantify HAD on 293T cell monolayers expressing the indicated HNs. The values are means (±SD) of results from three experiments. (B) 293T cells transiently expressing the indicated HN were allowed to bind RBCs at 4°C for 30 min at pH 5 and then transferred to 37°C. Percent RBCs released at 0, 5, 10, 15, 30, and 60 min were determined (*y* axis). Values are means (±SD) of results from triplicate wells. (C) 293T cells coexpressing the indicated HN-F pair were allowed to bind RBCs at 4°C and then transferred to 4, 15, 22, 30, or 37°C for 1 h. RBCs released, bound, and fused were quantified. Values are means (±SD) of results from three experiments.

temperature of F activation was considered to be the temperature at which there is 50% RBC fusion. HN wt required a temperature of 18°C to achieve 50% binding or fusion (Fig. 5C). HN H552Q, the most efficient at F triggering, required only 12°C (Fig. 3B). Introduction of Q559R into the parental HN H552Q increased the activation temperature to 31°C, while singly mutated HN Q559R

TABLE 2 Characteristics of variant HPIV3 HN and F proteins

Protein	Receptor avidity (mU for 50% RBC binding)	Neuraminidase level (% of HN wt level)	Release (% RBC released in 15 min at pH 5)	Temp of F activation (°C)	
				F wt	F G396D
HN wt	44	100	13	18	37
HN H552Q	54	79.5	0.7	12	29
HN H552Q,Q559R	19	62.2	44	31	>37
HN Q559R	17	34.4	47	37	>37

required a temperature of 37°C for 50% binding/fusion. The Q559R mutation confers a decrease in the efficiency of HN's F-triggering property.

It is conceivable that the F activation temperatures of HN H552Q,Q559R and HN Q559R might have been obscured by the significant release of RBCs during the fusion-triggering assay. To address this issue, we removed the neuraminidase activity of these HNs in order to evaluate simply the inherent F-triggering ability of the HNs. The mutation D216R, which abolishes neuraminidase activity without affecting binding or F activation (13), was introduced into HN H552Q,Q559R and HN Q559R. HN carrying the D216R mutation is irreversibly receptor engaged. The HN D216R,H552Q,Q559R construct did not produce a functional protein on the cell surface, but HN D216R,Q559R was expressed at levels comparable to those for all other HNs (data not shown). Using HN D216R,Q559R in the presence of F wt, the fusion-triggering assay revealed that even without release of RBCs during the fusion assay, the temperature of activation for HN D216R,Q559R was still 28°C (Fig. 5C). This suggested that HN Q559R was inherently less efficient at activating F relative to HN wt and HN H552Q, a result not explained simply by release of receptor-bearing cells prior to F activation.

Coevolution of HN and F in HAE identifies key characteristics required for HPIV3 growth in the lung. To achieve optimal growth characteristics in host tissue, the large-plaque HPIV3 HN H552Q virus underwent evolution to reduce the efficiency of its fusion machinery in several ways: by decreasing F's susceptibility to activation, by decreasing HN's receptor avidity, by decreasing HN's neuraminidase, and by decreasing HN's fusion-triggering capacity. The combination of characteristics led to diminished HN-F activation. Table 2 summarizes the individual characteristics of each protein in the series. The parent HPIV3 HN H552Q first acquired a mutation in F that impacted F's ability to be activated, but this mutation alone was insufficient for generating a stable virus. The introduction of Q559R into HN's site II resulted in a decrease in avidity, neuraminidase, and HN's F-triggering functions, producing a virus that is viable in the lung tissue.

TABLE 3 Flow cytometric analysis of HN cell surface expression by FACS analysis with anti-HN monoclonal antibody

Protein	No. of cell surface HN molecules/cell[a]
HN wt	91,200 ± 24,617
HN H552Q	90,041 ± 19,838
HN H552Q,Q559R	93,263 ± 14,342
HN Q559R	96,878 ± 12,439

[a] Data are representative of results from four experiments (averages ± SE).

DISCUSSION

Infection by HPIV3 in lung is an ongoing positive selection process in which the strength of binding to host cells, fusion activation, and receptor cleavage fluctuate until a stable balance is achieved. Our previous studies have shown that avid binding of HN to the host cell receptor, paired with efficient fusion activation by HN, was suited for infection and growth in monolayer culture but proved to be counterproductive in cotton rats and HAE (9). The studies reported here on the evolution of the virus in natural tissue, achieved through experiments that permit the HN/F fusion machinery to adapt in the natural host, explain the differences in outcomes in terms of specific HN-F activities over time.

A key factor for viral infection in the host is an HN that does not prematurely activate F before viral entry. Several viral properties contribute to this effect. In the lung, HPIV3 bearing an HN with lower avidity may be superior to one with a more avid HN because the resulting requirement for higher activation energy protects F from activation, delaying the triggering of F until the conditions are right for fusion. We have suggested (5, 9) that the correct timing of F activation is essential for viral entry and spread and that triggering should occur only when F is in proximity to the target cell membrane. HPIV3 HN H552Q produced noninfectious particles after primary infection of HAE (9), and we now have found that exposure to the selective pressure of growth in HAE favored the emergence of a new viral variant with slower fusion kinetics. It is possible that the generous availability of receptors in the lung could be the factor in HAE that caused HPIV3 HN H552Q viruses to be noninfectious after the primary infection. HN H552Q, avid for receptor binding and efficient at F activation, would result in these viruses binding to sialic acid-containing moieties in the lung, leading to premature activation of F. The virus that emerged under the selective pressure in HAE (HPIV3 HN H552Q,Q559R F G396D) carries an HN with lower avidity for receptor binding and less-efficient activation of F. This variant grows even better than our lab-adapted wt HPIV3 in the HAE. These slow fusion machinery characteristics may also be shared with HPIV3 clinical isolates; an analysis is ongoing. Specific fusion kinetics may be a key factor in long-term virus survival and growth *in vivo*.

The appearance and survival of the mutations in HN and F over time suggest several key characteristics of successful HN-F interactions. In host tissue, from a highly avid and fusogenic HPIV3 carrying HN H552Q, a new and unstable variant was positively selected with a mutated fusion protein that was less fusogenic than its predecessor. This unstable virus then acquired a second mutation in HN's secondary sialic acid binding site—Q559R—to form a stable and poorly fusogenic virus, which grew better in HAE than the HPIV3 wt virus that has been propagated in the laboratory. These findings suggest that the emergence of the less-fusogenic F protein mutant required changes in HN's site II to achieve a stable virus. Conversely, the mutations that were advantageous for growth in natural tissue led to poor growth in immortalized cells; infection of CV1 cells with HPIV3 HN H552Q,Q559R/F G396D led to the acquisition of new mutations in the glycoproteins and a change in plaque size and morphology (data not shown).

The H552 and Q559 residues are located at the HN dimer interface, near the second active site in the published X-ray crystal structure of HN (PDB 1V2I) (16) (Fig. 2A). The introduction of Q559R was the final step in the evolution from a virus unfit for growth in lung to a stable HPIV3 variant that is highly infectious in HAE. While the H552Q mutation confers higher avidity for receptors and increased F triggering relative to results for HN wt, the introduction of Q559R into the HN protein has the opposite effect. Q559R decreases HN's avidity for receptors as well as its ability to activate the F protein. Note that the HN surface expression levels do not differ between wt HN and mutants, including HN containing the Q559R mutation (Table 3). Using the published HN structure (above), the H552 residue was mutated to Q *in silico*. The mutation did not significantly alter the dimer interface or the local protein conformation. Based on this modeling

and molecular dynamics simulation, the 552Q mutation does not seem to disrupt and might in fact strengthen the interaction and participates in intermolecular hydrogen binding; this could account for our recent biochemical data showing that H552Q alters dimerization of HN (10).

The second mutation at this site, Q559R, might disrupt the dimer observed in the crystal structure. The arginines facing each other, in addition to not fitting into the tight space at the dimer interface, could create charge repulsion, possibly disrupting the dimer. However, generating this mutation *in silico* is not possible because the dimer interface of the currently available crystal structure of HN (16) does not permit this mutation. Additional structural analysis will explore the effects of this mutation on HN.

The residue mutated in the F protein, glycine 396, is located on a long loop of F's domain II, which is surface exposed both in the postfusion crystal structure (PDB 1ZTM) (17) and in a homology model of the prefusion structure (model based on the parainfluenza virus 5 [PIV5] F protein, PDB 2B9B) (18) (Fig. 2B). The G396D position is accessible and remains in the same structural location in the pre- and postfusion conformations of F. The mutation confers slower triggering kinetics on the protein, indicating that this domain is involved in the triggering mechanism. While in our study the mutation in F emerged to permit growth in lung tissue, several experiments using site-directed mutagenesis in other paramyxoviruses have shown that mutations in this domain of F can modulate F activation, most likely by stabilizing the prefusion state (19–21). Of note, this residue is the same location on F that was targeted by the effective prophylactic monoclonal antibody for respiratory syncytial virus, supporting the notion that this location is a key functional region that is preserved between paramyxovirus F proteins (22, 23).

The progressive evolution from the parental HPIV3 HN H552Q to HPIV3 HN H552Q,Q559R/F G396D, from larger to smaller plaques and to decreased F triggering, highlights the disadvantage of the parental virus' fusion machinery. The HN-F machinery of HPIV3 HN H552Q, to adapt to the lung tissue, evolved to decrease its F activation capacity first, to grow in HAE, and a second mutation in HN's second sialic acid binding site, decreasing avidity and HN's F activation, conferred optimal growth in the airway cultures. The results support the role of HN's sialic acid binding site II in controlling F activation and underscore the notion that timely F activation is required for infection in host tissue. The HN-F pair of the HAE fit virus requires more energy to initiate fusion. In distinction from the features that confer fusogenicity in monolayer cultures, a virus carrying an HN with low receptor avidity, a high rate of release from the receptor, and decreased efficiency of activating the F protein and with reduced fusion is fit for growth in the natural host.

The mechanisms underlying HN-F activity offer opportunities for subverting the viral fusion process. Apart from inhibiting viral entry, it may be possible to force viral evolution towards developing HN host receptor binding that is strong enough to prematurely activate F and circumvent fusion. Recently, we identified compounds that stimulate HPIV3 HN to trigger F prematurely, before the virus contacts the target cell membrane, and thereby inactivate infectivity in HAE (5). Such compounds are of potential significance as antiparamyxovirus therapies and should be highly unlikely to elicit resistance mutations. Mutants arising under the selective pressure of premature-triggering compounds would have fusion machineries that are too impaired for viability and would thus be less fit and transmissible than the parent virus. Virions harboring mutations in their fusion machinery that would make them resistant to prematurely activating compounds would therefore be likely to be unresponsive in physiological situations, rendering them less fit to infect and cause disease. Characterizing molecular attributes of HN and F as well as the timing, kinetics, and interaction between HN and F as a complex in lung tissue allows us to consider the HN-F fusion machinery with its various components in balance, as a biological complex, tuned for survival in the host.

MATERIALS AND METHODS

Human airway epithelial cultures. The EpiAirway AIR-100 system (MatTek Corporation) consists of normal, human-derived tracheobronchial epithelial cells that have been cultured to form a pseudostratified, highly differentiated mucociliary epithelium. Upon receipt from the manufacturer, HAE cultures were handled as previously described (9, 12).

Monolayer cells. CV-1 (African green monkey kidney) and 293T (human kidney epithelial) cells were grown in Dulbecco's modified Eagle's medium (Cellgro; Mediatech) supplemented with 10% fetal bovine serum and antibiotics at 37°C in 5% CO_2.

Viruses. Titers of HPIV3 virus stocks were assessed by a plaque assay (9, 12). Supernatant fluids collected from HAE were used to infect CV-1 cells. Isolated plaques were enclosed in a 1-mm-diameter plastic cylinder, and trypsin was added to disrupt the plaque. Complete medium (100 μl) was then added, and the mixture was collected. This fluid was then used to infect HAE recurrently to ensure that the plaque retained its morphology over 2 to 3 passages for preparation of viral stocks.

RNA isolation and sequence analysis of HN and F genes. Total RNA was isolated from CV1 cells infected with plaque-purified virus or supernatant fluids collected from HAE or the HAE cultures themselves, infected with 4,000 PFU of HPIV3 WT or the variant viruses. RNA isolation and sequencing were performed as previously described, and sequence analysis was carried out on the DNA products of three separate isolations and performed twice on all samples to confirm sequence alterations (24, 25).

qRT-PCR. To measure the amount of viral genome released, 30 μl of fluid containing released virus was processed for RNA extraction, and then the genome was quantified using the real-time one-step qRT-PCR pathogen detection kit specific for HPIV3 (PrimerDesign) as per the manufacturer's instructions.

Modeling of HN and F and molecular dynamics simulation. For molecular dynamics (MD) simulation, the wt or H552Q mutant HN was solvated in a water box extending 10 Å in all directions beyond the edge of the protein, using the TIP3P water model z (26, 27). The system was neutralized with a 150 mM concentration of sodium/chloride ions and consisted of a total of 66,000 atoms. Mutagenesis and system preparation was performed with the VMD software program (28). MD calculations were performed with the NAMD program (29) using the CHARMM27 force field. The systems were energy minimized with 10,000 steps of conjugate gradient energy minimization, followed by gradual heating from 0 to 310 K in 30 ps, and then maintained at constant temperature and pressure (1.01325×10^5 Pa). The simulations were carried out with periodic box conditions, with a 2-fs time step, a uniform dielectric constant of 1, a 1 to 4 scaling value of 1.0, a cutoff of nonbonded forces with a switching function starting at 10 Å and reaching 0 at 12 Å, particle mesh Ewald (PME) with a tolerance of 10^{-6}, and all bonds involving hydrogens constrained with the SHAKE algorithm. A production run was performed for 20 ns, and the trajectories were analyzed with VMD.

The structure of the prefusion F protein from HPIV3 was homology modeled using the HHpred server (http://toolkit.tuebingen.mpg.de/hhpred#) and the parainfluenza virus 5 (PIV5) structure as the template (18).

Measuring plaque size. Plaque diameter was measured at a magnification of 15× under a zoom stereomicroscope equipped with a microme-

ter. Surface area calculations from 20 plaques were used to establish mean plaque areas with standard deviations.

HN and F constructs and transient expression. Cloned HPIV3 HN variant cDNAs were digested with EcoRI and BamHI and ligated into a digested pEGFP-C3 vector (BD Biosciences/Clontech). Cloned HPIV3 F cDNAs were digested with XhoI and BamHI and ligated into digested pCAGGS mammalian expression vectors. Positive clones were sequenced to verify the mutations and to ensure that no additional alterations had been introduced. Transfections were performed according to the Lipofectamine Plus or Lipofectamine 2000 manufacturer's protocols (Invitrogen).

Assay of neuraminidase activity. Monolayers of 293T cells transiently expressing WT or mutant HNs were washed once with phosphate-buffered saline (PBS) and then incubated for 10 min in 5 mM EDTA in 1× PBS put in pH 5.0 CO_2-independent medium (Gibco). Cells (150,000) were transferred to 96-well plates and incubated at 37°C for 10 min. 2′-(4-Methylumbelliferyl)-a-d-*N*-acetylneuraminic acid sodium salt (MUNANA) (20 mM; Toronto Research Chemical) was added at 1:1 (vol/vol) for a final concentration of 10 mM MUNANA. A kinetic reading at 37°C was done using a SpectraMax M5 enzyme-linked immunosorbent assay (ELISA) reader every 2 min for 1 h.

Use of receptor-depleted RBCs to assess HN receptor-binding avidity. Human RBCs were obtained from healthy donors as previously described (24). Partial receptor depletion of RBCs was carried out, and RBCs which were partially depleted of their surface sialic acid receptors were used to determine the relative receptor binding avidities of variant HN molecules as described previously (7, 13).

Assays for F activation, receptor retention, and receptor release. Monolayers of 293T cells transiently expressing F wt or mutant or HN wt or mutant were washed three times and incubated with 1% RBC suspensions at pH 7.3 for 30 min at 4°C. After rinsing to remove unbound RBCs, the plates were transferred to 4, 15, 22, 30, or 37°C for 1 h. After this incubation, RBCs that were released to the medium, remained bound, or had undergone membrane fusion were quantified as described previously (7, 13).

***β*-Galactosidase complementation-based fusion assay.** The *β*-galactosidase complementation-based fusion assay was performed as previously described (7, 13, 32).

Cell surface expression assay. Monolayers of 293T cells were transfected for transient expression of HN or F constructs. Cells were washed twice in PBS and then incubated with an anti-HPIV3 HN monoclonal antibody supplied by Judy Beeler in 3% bovine serum albumin (BSA), 0.1% sodium azide in PBS for 1 h. Samples were then washed twice in PBS and incubated with 1:100 anti-mouse IgG (H+L) R-phycoerythrin conjugate (Caltag Laboratories). To quantify the amounts of cell surface proteins in each sample, an indirect immunofluorescence assay was used, where beads from the Qifikit kit (Dako) were stained simultaneously with samples according to manufacturer's instructions, with the same secondary antibody. Cell surface expression of all samples and beads was performed with fluorescence-activated cell sorting (FACS) (FACSCalibur; Becton, Dickinson) (10, 30, 31).

ACKNOWLEDGMENTS

We are grateful to Ashton Kutcher and Jonathan Ledecky for their microscopy support, to Dan and Nancy Paduano for their essential support of innovative research projects, and to the Friedman Family Foundation for our laboratories at Weill Cornell Medical College. We thank Tim McGraw for helpful scientific discussions and advice, Eric M. Jurgens for help with statistical analysis, and Christine C. Yokoyama for critical reading of the manuscript. We acknowledge the flow cytometry support from Sergei Rudchenko in the Flow Cytometry Facility of the Hospital for Special Surgery/Weill Cornell Medical College. Computations were performed on the David A. Cofrin computational infrastructure of the Institute for Computational Biomedicine at Weill Cornell Medical College.

The work was supported by NIH grant R01AI31971 to A.M. and NIH grant 3R01AI031971-19S1 (Research Supplement to Promote Diversity in Health-Related Research Program) to A.M.

REFERENCES

1. **Henrickson KJ, Hoover S, Kehl KS, Hua W.** 2004. National disease burden of respiratory viruses detected in children by polymerase chain reaction. Pediatr. Infect. Dis. J. **23**:S11–S18.
2. **Moscona A.** 2005. Entry of parainfluenza virus into cells as a target for interrupting childhood respiratory disease. J. Clin. Invest. **115**: 1688–1698.
3. **Srinivasan A, et al.** 2011. Symptomatic parainfluenza virus infections in children undergoing hematopoietic stem cell transplantation. Biol. Blood Marrow Transplant. **17**:1520–1527.
4. **Yang HT, et al.** 2011. Identification of a natural human serotype 3 parainfluenza virus. Virol. J. **8**:58.
5. **Farzan SF, et al.** 2011. Premature activation of the Paramyxovirus fusion Protein before target cell attachment with corruption of the viral fusion machinery. J. Biol. Chem. **286**:37945–37954.
6. **Moscona A, Peluso RW.** 1993. Relative affinity of the human parainfluenza virus type 3 hemagglutinin-neuraminidase for sialic acid correlates with virus-induced fusion activity. J. Virol. **67**:6463–6468.
7. **Porotto M, Fornabaio M, Kellogg GE, Moscona A.** 2007. A second receptor binding site on human parainfluenza virus type 3 hemagglutinin-neuraminidase contributes to activation of the fusion mechanism. J. Virol. **81**:3216–3228.
8. **Porotto M, et al.** 2004. Inhibition of parainfluenza virus type 3 and Newcastle disease virus hemagglutinin-neuraminidase receptor binding: effect of receptor avidity and steric hindrance at the inhibitor binding sites. J. Virol. **78**:13911–13919.
9. **Palermo LM, et al.** 2009. Human parainfluenza virus infection of the airway epithelium: viral hemagglutinin-neuraminidase regulates fusion protein activation and modulates infectivity. J. Virol. **83**:6900–6908.
10. **Porotto M, Palmer SG, Palermo LM, Moscona A.** 2012. Mechanism of fusion triggering by human parainfluenza virus type III: communication between viral glycoproteins during entry. J. Biol. Chem. **287**:778–793.
11. **Zhang L, et al.** 2005. Infection of ciliated cells by human parainfluenza virus type 3 in an *in vitro* model of human airway epithelium. J. Virol. **79**:1113–1124.
12. **Moscona A, et al.** 2010. A recombinant sialidase fusion protein effectively inhibits human parainfluenza viral infection *in vitro* and *in vivo*. J. Infect. Dis. **202**:234–241.
13. **Palermo LM, Porotto M, Greengard O, Moscona A.** 2007. Fusion promotion by a paramyxovirus hemagglutinin-neuraminidase protein: pH modulation of receptor avidity of binding sites I and II. J. Virol. **81**: 9152–9161.
14. **Connolly SA, Leser GP, Jardetzky TS, Lamb RA.** 2009. Bimolecular complementation of paramyxovirus fusion and hemagglutinin-neuraminidase proteins enhances fusion: implications for the mechanism of fusion triggering. J. Virol. **83**:10857–10868.
15. **Connolly SA, Leser GP, Yin HS, Jardetzky TS, Lamb RA.** 2006. Refolding of a paramyxovirus F protein from prefusion to postfusion conformations observed by liposome binding and electron microscopy. Proc. Natl. Acad. Sci. U. S. A. **103**:17903–17908.
16. **Lawrence MC, et al.** 2004. Structure of the haemagglutinin-neuraminidase from human parainfluenza virus type III. J. Mol. Biol. **335**:1343–1357.
17. **Yin HS, Paterson RG, Wen X, Lamb RA, Jardetzky TS.** 2005. Structure of the uncleaved ectodomain of the paramyxovirus (hPIV3) fusion protein. Proc. Natl. Acad. Sci. U. S. A. **102**:9288–9293.
18. **Yin HS, Wen X, Paterson RG, Lamb RA, Jardetzky TS.** 2006. Structure of the parainfluenza virus 5 F protein in its metastable, prefusion conformation. Nature **439**:38–44.
19. **Lee JK, et al.** 2008. Functional interaction between paramyxovirus fusion and attachment proteins. J. Biol. Chem. **283**:16561–16572.
20. **Schowalter RM, Chang A, Robach JG, Buchholz UJ, Dutch RE.** 2009. Low-pH triggering of human metapneumovirus fusion: essential residues and importance in entry. J. Virol. **83**:1511–1522.
21. **Smith EC, Dutch RE.** 2010. Side chain packing below the fusion peptide strongly modulates triggering of the Hendra virus F protein. J. Virol. **84**: 10928–10932.

22. **McLellan JS, Yang Y, Graham BS, Kwong PD.** 2011. Structure of respiratory syncytial virus fusion glycoprotein in the postfusion conformation reveals preservation of neutralizing epitopes. J. Virol. **85**:7788–7796.
23. **Swanson KA, et al.** 2011. Structural basis for immunization with postfusion respiratory syncytial virus fusion F glycoprotein (RSV F) to elicit high neutralizing antibody titers. Proc. Natl. Acad. Sci. U. S. A. **108**:9619–9624.
24. **Murrell MT, Greengard O, Porotto M, Poltoratskaia N, Moscona A.** 2001. A single amino acid alteration in the human parainfluenza virus type 3 hemagglutinin-neuraminidase glycoprotein confers resistance to the inhibitory effects of zanamivir on receptor binding and neuraminidase activity. J. Virol. **75**:6310–6320.
25. **Murrell M, Porotto M, Weber T, Greengard O, Moscona A.** 2003. Mutations in human parainfluenza virus type 3 hemagglutinin-neuraminidase causing increased receptor binding activity and resistance to the transition state sialic acid analog 4-GU-DANA (zanamivir). J. Virol. **77**:309–317.
26. **Jorgensen WL.** 2004. The many roles of computation in drug discovery. Science **303**:1813–1818.
27. **Jorgensen WL, Maxwell DS, Tirado-Rives J.** 1996. Development and testing of the OPLS all-atom force field on conformational energetics and properties of organic liquids. J. Am. Chem. Soc. **118**:11225–11236.
28. **Humphrey W, Dalke A, Schulten K.** 1996. VMD: visual molecular dynamics. J. Mol. Graph. **14**:33–38, 27–38.
29. **Phillips JC, et al.** 2005. Scalable molecular dynamics with NAMD. J. Comput. Chem. **26**:1781–1802.
30. **Latger-Cannard V, et al.** 2000. [Use of standard for quantitation of adhesion of polynuclear neutrophils by flow cytometry]. Ann. Biol. Clin. (Paris) **58**:337–343.
31. **Smith KB, Ellis SA.** 1999. Standardisation of a procedure for quantifying surface antigens by indirect immunofluorescence. J. Immunol. Methods **228**:29–36.
32. **Moosmann P, Rusconi S.** 1996. Alpha complementation of LacZ in mammalian cells. Nucleic Acids Res. **24**:1171–1172.